

RefVSR++: Exploiting Reference Inputs for Reference-based Video Super-resolution

Han Zou^{1,2} Masanori Suganuma^{1,2} Takayuki Okatani^{1,2}

¹Graduate School of Information Sciences, Tohoku University ²RIKEN Center for AIP

{hzou, suganuma, okatani}@vision.is.tohoku.ac.jp

Abstract

Smartphones equipped with a multi-camera system comprising multiple cameras with different field-of-view (FoVs) are becoming more prevalent. These camera configurations are compatible with reference-based SR and video SR, which can be executed simultaneously while recording video on the device. Thus, combining these two SR methods can improve image quality. Recently, Lee et al. have presented such a method, RefVSR. In this paper, we consider how to optimally utilize the observations obtained, including input low-resolution (LR) video and reference (Ref) video. RefVSR extends conventional video SR quite simply, aggregating the LR and Ref inputs over time in a single bi-directional stream. However, considering the content difference between LR and Ref images due to their FoVs, we can derive the maximum information from the two image sequences by aggregating them independently in the temporal direction. Then, we propose an improved method, RefVSR++, which can aggregate two features in parallel in the temporal direction, one for aggregating the fused LR and Ref inputs and the other for Ref inputs over time. Furthermore, we equip RefVSR++ with enhanced mechanisms to align image features over time, which is the key to the success of video SR. We experimentally show that RefVSR++ outperforms RefVSR by over 1dB in PSNR, achieving the new state-of-the-art.

1. Introduction

Recent mobile phones are now equipped with multiple cameras, typically two or three, to enhance the overall photography experience. The equipped cameras have different focal lengths, allowing users to capture photos/videos with different fields of view (FoVs) simultaneously. For example, in a scenario where two cameras with different FoVs capture the same scene, the camera with a narrower FoV produces a higher-resolution image of the corresponding portion of the scene. Integrating it with the same scene

image captured by the other camera with a larger FoV will allow us to increase its image resolution, at least in the region of overlap between the FoVs.

This problem, known as reference-based image super-resolution (Ref-SR), has been studied recently in the community, resulting in the development of several methods [12, 17, 9, 24, 19, 22, 23]. It is formalized as predicting a high-resolution SR image of a low-resolution (LR) input of a scene, aided by a reference (Ref) image of a similar scene. Specifically, we consider a scenario where the Ref image has a narrower FoV than the LR image. Existing Ref-SR methods first find the correspondences between the LR and Ref images, followed by warping the Ref image to align with the LR image, and finally fusing them to predict higher quality SR images.

When taking a video, not a single photograph, of a scene with mobile phone cameras, we can increase the image resolution in a different way by using the images contained in the video. It is to aggregate the images in the temporal axis and obtain a rich visual feature of the captured scene, from which we super-resolve each image. Note that this is doable even with a single camera. This is called video SR (VSR), which has also been studied for a while in the community.

Now, with mobile phones equipped with multiple cameras, it is possible to integrate VSR with reference-based super-resolution (Ref-SR) to further enhance the quality of super-resolved images. Recently, Lee et al. [12] have proposed a method for this problem, reference-based video SR, named RefVSR. While RefVSR has shown promising results, we believe there is much room for further improvements.

There are two key issues with reference-based video SR. The first pertains to how to make maximum use of all available observations. Specifically, given a sequence of LR images and a sequence of Ref images, conventional video SR methods can effectively handle the LR image sequence since their objective is to super-resolve them. However, this may not apply to the Ref images. An arbitrary number of Ref images at arbitrary time steps could provide valuable information to super-resolve an LR image at a particular time

step. Then, it will be crucial to determine the most useful Ref image(s) and aggregate them for the LR image at each time step.

The second is how to match and align images accurately. Reference-based video SR requires aligning images over time and aligning the LR and Ref images at each time step. The former is a fundamental requirement of a well-established video SR approach, which propagates image features over time to generate high-quality SR images. However, the propagation is susceptible to the accumulation of errors, which causes a misalignment of images, leading to blurry SR outputs. We point out that existing methods for image alignment are error-prone.

Based on these considerations, we propose a novel method for reference-based video SR dubbed RefVSR++. It extends RefVSR, resolving the aforementioned critical issues. First, RefVSR++ is designed to maximize the use of both the Ref and LR image sequences. Specifically, RefVSR++ utilizes two streams to propagate different image features, in contrast to RefVSR which uses only one. One stream propagates the features of Ref images, referred to as the Ref feature stream, and the other propagates aggregated Ref and LR image features, referred to as the SR feature stream. Information flows unidirectionally from the Ref feature stream to the SR feature stream. Both streams propagate features in a recurrent and bi-directional manner as with RefVSR.

Second, RefVSR++ addresses the issue of image alignment by utilizing a more accurate and robust method than the confidence-guided method used in RefVSR. To achieve this, we combine deformable convolution with the standard image alignment method based on optical flow estimation. Additionally, We propose a learning-free method for propagating more reliable Ref features. Specifically, it replaces low-confidence Ref features with high-confidence ones in the Ref image sequence.

These component methods extend RefVSR and enable more effective feature aggregation across all input images over an extended period of time, leading to superior SR outputs. The resultant method, RefVSR++, has established the new state-of-the-art on the RealMVCVR dataset, i.e., PSNR/SSIM = 35.90/0.965 (RefVSR++) vs. 34.86/0.959 (RefVSR).

2. Related Work

2.1. Video Super-Resolution

The goal of video super-resolution (VSR) is to recover a high-resolution (HR) video from a low-resolution (LR) input video. VSR has been studied for a long time. Recent methods are classified into two categories: methods based on a sliding window and those based on recurrent computation. The sliding window is widely used in CNN-based

VSR methods [15, 25, 13, 16, 18, 11], which receive several consecutive frames as input, traverse them with a sliding window, and then predict an SR image of their center frame. These methods must process each frame multiple times to handle a long video. Thus, they tend to suffer from a high computational cost, and they can deal with a limited number of input frames, which makes it hard to deal with long-term dependencies. Methods based on recurrent computation [8, 10, 6, 3, 4, 14] utilize reconstructed high-quality images at previous time steps or their features to generate high-quality images at the current time step. Huang et al. [8] propose recurrent bi-directional networks to better utilize temporal information. Chan et al. [4] propose using high-order grid connections and flow-guided alignment for the recurrent computation.

2.2. Reference-based Super-Resolution

Reference-based super-resolution (RefSR) uses additional reference image(s) to super-resolve an input low-resolution image. Previous studies have shown the effectiveness of transferring information from a high-resolution reference image to generate SR images. A critical problem is accurately aligning the Ref image with the LR image, which is important for fusing their image features in a subsequent step to generate high-quality SR images. Zheng et al. [24] estimate optical flows between them for their alignment. Zhang et al. [22] propose using patch matching [1], and Yang et al. [20] improve it by adopting attention mechanisms for feature fusion. Wang et al. [17] propose an aligned attention method for better feature fusion, which preserves high-frequency features via spatial alignment operations well. Huang et al. [9] decouple ref-based SR task into two sub-tasks: single image SR task and texture transfer task, and train them independently. It reduces misuse and underuse of the Ref feature, which often happens in Ref feature transfer. Lee et al. [12] propose RefVSR, which integrates RefSR with VSR; we will discuss their method in detail below.

3. Improved Use of References for VSR

3.1. Problem Formulation and Notation

Let $I_t^{LR} (\in \mathbb{R}^{H \times W \times C})$ be an input sequence of low-resolution images, and $I_t^{Ref} (\in \mathbb{R}^{H \times W \times C})$ be an input sequence of reference images, with $t = 1, \dots, T$. Here, H, W, C are the size/number of height, width, and channels of the images, respectively. Note that I_t^{LR} is a low-resolution image of a scene with a large FoV; I_t^{Ref} is an image of the same scene with a narrow FoV, making it a higher-resolution image of a part of the scene; see Fig. 8. The goal is to generate a SR version $I_t^{SR} (\in \mathbb{R}^{sH \times sW \times C})$ of I_t^{LR} with an upscaling factor s .

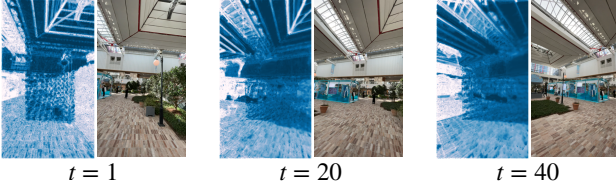


Figure 1: Examples of a propagated confidence map (left) and an input LR frame (right) at different time steps.

3.2. Revisiting RefVSR

RefVSR [12] integrates reference-based SR and video SR to solve the above problem. For the former, RefVSR uses I_t^{Ref} by warping and fusing its feature f_t^{Ref} with the feature f_t^{LR} of I_t^{LR} [20, 22, 24, 17]. For the latter, RefVSR propagates scene image feature h_t in a recurrent fashion with $t = 1, \dots, T$ [7, 8, 6, 3, 4], where h_{t-1} from the previous time step is aligned with the current feature f_t^{LR} to compensate for the motion from $t-1$ to t , and then fused with f_t^{LR} to obtain an enriched feature h_t generating a high-quality SR image I_t^{SR} ; see Fig. 2(a). RefVSR adopts bidirectional recurrent propagation in the forward (i.e., $t-1$ to t) and backward (i.e., $t+1$ to t) directions, following recent studies [3, 4, 8].

The computation in each recurrent cell is as follows. It first warps the Ref image feature f_t^{Ref} and the propagated feature h_{t-1} from the previous step into \tilde{f}_t^{Ref} and \tilde{h}_{t-1} to align them with f_t^{LR} . It computes a confidence map for the alignment of \tilde{f}_t^{Ref} with f_t^{LR} . It also propagates and updates another confidence map for the alignment of \tilde{h}_{t-1} with f_t^{LR} , and then fuses \tilde{f}_t^{Ref} and \tilde{h}_{t-1} with f_t^{LR} to produce h_t . Here, it employs a confidence-guided fusion to select well-matched features from \tilde{f}_t^{Ref} using the above confidence map, and well-matched features from \tilde{h}_{t-1} using the propagated confidence map.

There exist two drawbacks to this approach. First, **it does not derive all the information from the inputs**. That is, we have two observations I_t^{Ref} and I_t^{LR} at each time step t . RefVSR propagates only one type feature h_t in the temporal domain, which fuses and accumulates I_t^{Ref} and I_t^{LR} ; see Fig. 2(a). However, I_t^{Ref} and I_t^{LR} contain different information due to their FoVs. For example, since the warped Ref feature \tilde{f}_t^{Ref} is aligned with f_t^{LR} , its feature outside the overlapped FoV can be error-prone. It is ideal that we propagate two features independently for I_t^{Ref} and I_t^{LR} .

Second, **RefVSR propagates a confidence map along with h_t over time, which is not well-founded compared to other components**. Although the motivation is to select well-matched features for feature fusion, the method updating the confidence map appears heuristic; it takes the maximum of the flow warped propagated confidence map and the confidence map of the alignment of f_t^{Ref} and f_t^{LR} .

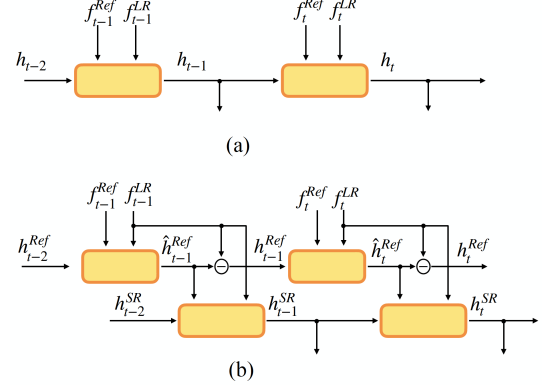


Figure 2: Comparison of (a) RefVSR and (b) RefVSR++(ours). While RefVSR propagates only a single feature, ours propagates two features to aggregate all available information over time. For simplicity, only the forward propagation is shown and the confidence map that RefVSR propagates is omitted.

However, the estimated optical flow is suboptimal and errors accumulate during repeated spatial warping, thereby jeopardizing the accuracy of Ref feature fusion.

We show an example of a long-term backward propagation of Ref-based VSR in Fig 1, which shows the input LR sequences and the warped propagated confidence maps. We can see that confidence maps gradually become blurry over time, which will deteriorate the quality of feature fusion; see also Sec. 5.3.

3.3. Proposed Approach

Based on the above considerations, we propose to independently propagate features of I_t^{Ref} and I_t^{LR} , as shown in Fig. 2(b). As the goal is to generate I_t^{SR} from the feature propagation, we choose to propagate, not their features themselves, but one feature for I_t^{Ref} and the *fused* Ref and LR feature, from which we generate I_t^{SR} . We also cease to propagate a confidence map.

Specifically, we propagate the fused Ref and LR feature, denoted by h_t^{SR} since it yields I_t^{SR} , and also the Ref feature, denoted by h_t^{Ref} . Strictly, we propagate the residual of the learned feature, i.e., $h_t^{Ref} \equiv \hat{h}_t^{Ref} - f_t^{LR}$, where \hat{h}_t^{Ref} is the Ref feature. Following the RefVSR and recent VSR methods, we employ bidirectional streams for the recurrent updates of the feature.

4. Details of the Proposed Method

4.1. Overview

Figure 3 shows the overview of the proposed network. As also shown in Figs. 2(b), it has two recurrent cells that propagate and update h^{Ref} and h^{SR} in each of the forward

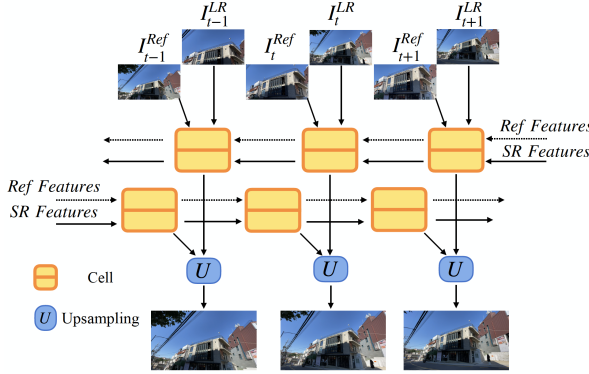


Figure 3: Overview of the proposed method. I_t^{LR} and I_t^{Ref} are inputted into all recurrent cells in forward and backward directions. The arrows to the cells in the forward stream are omitted for brevity.

and backward streams and a single module that fuses the two h^{SR} 's from the two streams and generates I^{SR} . The latter is merely an upsampling module consisting of Res-Blocks and pixel shuffle as in RefVSR.

We use forward propagation for an explanation below and omit the backward propagation since we do the same for it in the opposite direction. In each recurrent cell, we first extract the feature f_t^{LR} and f_t^{Ref} from I_t^{LR} and I_t^{Ref} using two encoders, respectively.

4.2. Updating Ref Features

Figure 4 shows the recurrent cell for the Ref feature stream. The cell updates h_t^{Ref} as follows:

$$h_t^{Ref} = \hat{h}_t^{Ref} - f_t^{LR}, \quad (1a)$$

$$\hat{h}_t^{Ref} = F^{Ref}(h_{t-1}^{Ref}; f_t^{Ref}, f_t^{LR}, s_{t-1,t}), \quad (1b)$$

where $s_{t-1,t}$ is the optical flow from I_{t-1}^{LR} to I_t^{LR} estimated by a flow estimator.

It first warps h_{t-1}^{Ref} to compensate for the motion of the frame from $t-1$ to t . Following RefVSR, we estimate and use the optical flow $s_{t,t-1}$ to warp h_{t-1}^{Ref} to align with I_t^{LR} . Let \check{h}_{t-1}^{Ref} be the resulting feature.

However, the warped feature \check{h}_{t-1}^{Ref} tends to result in misalignment due to errors in the estimated flow $s_{t-1,t}$. As we want to propagate sharp textures from the Ref frames, we need more fine-grained alignment. Huang et al.[9] show the effectiveness of the combination of optical flow and deformable convolution (DCN) [4] for Ref feature alignment. Thus, adopting their approach, we employ DCN as follows:

$$\bar{h}_{t-1}^{Ref} = \mathcal{D}^{Ref}(\check{h}_{t-1}^{Ref}, o^{Ref}, m^{Ref}), \quad (2)$$

where o^{Ref} is offset for the estimated optical flow and

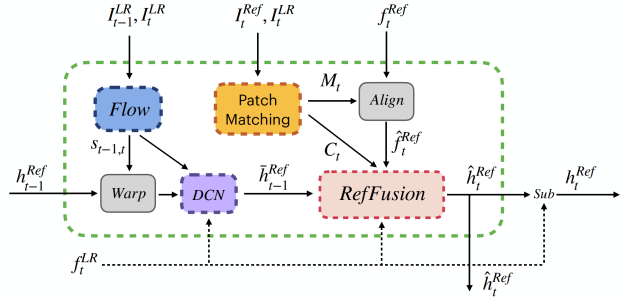


Figure 4: The recurrent cell for the Ref feature stream

m^{Ref} is a modulation mask, which are computed as

$$o^{Ref} = C_o^{Ref}([f_t^{LR}, \check{h}_{t-1}^{Ref}]) + s_{t-1,t}, \quad (3a)$$

$$m^{Ref} = \sigma(C_m^{Ref}([f_t^{LR}, \check{h}_{t-1}^{Ref}])), \quad (3b)$$

where C_o^{Ref} and C_m^{Ref} are convolutional layers and σ is a sigmoid function. We then align f_t^{Ref} with f_t^{LR} to compensate for the FoV difference in an adaptive fashion depending on the images' contents. We employ *patch matching*, following RefVSR and other earlier studies [12, 17, 9]. It is proven to be better for warping Ref features than optical flow-based warping. Specifically, it computes an index map M_t with its confidence map C_t for alignment as

$$\{M_t, C_t\} = Match(I_t^{LR}, I_t^{Ref}). \quad (4)$$

Specifically, we first embed I_t^{Ref} and I_t^{LR} into feature maps and extract 3×3 patches with a stride 1 using a shared encoder. Then we calculate the cosine distance $S_{i,j}$ between pairs of the LR feature patch i and the Ref feature patch j . The matching index and its confidence for patch i is given by $M_{t,i} = \arg \max_j S_{i,j}$ and $C_i = \max_j S_{i,j}$, respectively.

Finally, we warp f_t^{Ref} to \hat{f}_t^{Ref} using the index map M_t .

We then update the propagated Ref feature \bar{h}_{t-1}^{Ref} with the warped Ref feature \hat{f}_t^{Ref} . There are two potential issues with fusing such Ref features from different time steps. First, they may have different sharp textures at the same position due to the change of depth of field or illumination. Second, they contain different reliable regions. Thus, their direct fusion may result in a mismatch or blurred feature. To obtain a sharp fused Ref feature and preserve information from the current and previous Ref frames, we selectively transfer textures from the two Ref features \bar{h}_{t-1}^{Ref} and \hat{f}_t^{Ref} to the LR feature.

Specifically, we fuse each of \bar{h}_{t-1}^{Ref} and \hat{f}_t^{Ref} with the current frame's LR feature f_t^{LR} separately, aiming to preserve textures from the Ref features from different sources.

$$\tilde{h}_t^{Ref} = Conv([f_t^{LR}, \bar{h}_{t-1}^{Ref}], \quad (5a)$$

$$\hat{h}_t^{Ref} = Conv(C_t) \cdot Conv(f_t^{LR}, \hat{f}_t^{Ref}). \quad (5b)$$

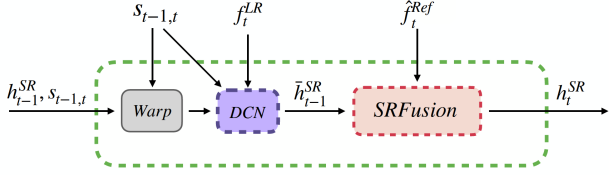


Figure 5: The recurrent cell for the SR feature stream

where $Conv$ is a convolutional layer. We adopt an adaptive fusion guided by the confidence map C_t to fuse \hat{f}_t^{Ref} . We then get the Ref feature by fusing the two Ref features obtained above.

$$\hat{h}_t^{Ref} = \mathcal{R}(\hat{h}_t^{Ref}, \tilde{h}_t^{Ref}, f_t^{LR}). \quad (6)$$

where \mathcal{R} is ResBlocks. We use \hat{h}_t^{Ref} to refine the propagated SR feature in the SR feature cell. Finally, we obtain the residual Ref feature as in (1a), which will be propagated to the next time step.

4.3. Updating SR Features

Figure 5 shows the recurrent cell for the SR feature stream. The cell updates the propagated SR feature using the Ref feature \hat{h}_t^{Ref} computed above and the current LR feature f_t^{LR} as

$$h_t^{SR} = F^{SR}(h_{t-1}^{SR}, \hat{h}_t^{Ref}, f_t^{LR}, s_{t-1,t}). \quad (7)$$

First, we align the propagated LR feature h_{t-1}^{SR} to the LR feature of the current time step t . Similarly to the Ref feature cell, we first warp it with the estimated flow $s_{t-1,t}$ and then apply deformable convolution to cope with possible misalignment. Letting \check{h}_{t-1}^{SR} be the warped feature by $s_{t-1,t}$, we apply DCN as

$$\check{h}_{t-1}^{SR} = \mathcal{D}^{SR}(\check{h}_{t-1}^{SR}, o^{SR}, m^{SR}), \quad (8)$$

with offset o^{SR} of flows and a modulation mask m^{SR} , which are given by

$$o^{SR} = C_o^{SR}(\hat{h}_t^{Ref}, \check{h}_{t-1}^{SR}) + s_{t-1,t}, \quad (9a)$$

$$m^{SR} = \sigma(C_m^{SR}(\hat{h}_t^{Ref}, \check{h}_{t-1}^{SR})), \quad (9b)$$

where C_o^{SR} and C_m^{SR} are convolutional layers and σ is a sigmoid function.

Next, we fuse the aligned feature \check{h}_{t-1}^{SR} with the updated Ref feature \hat{h}_t^{Ref} from the other cell using several ResBlocks as

$$h_t^{SR} = \mathcal{R}(\hat{h}_t^{Ref}, \check{h}_{t-1}^{SR}) + \check{h}_{t-1}^{SR}. \quad (10)$$

The resulting h_t^{SR} will be used to generate SR output at the current time step t and also propagated to the next time step.

4.4. Training

We use the RealMCVSR dataset [12] in our experiments. It consists of ultra-wide, wide-angle, and telephoto videos from multiple scenes. The three videos have the same size but different FoVs. Note that the wide and telephoto videos have twice ($2\times$) and four times ($4\times$) the magnification of the ultra-wide video, respectively. Following the paper [12], we consider the $4\times$ super-resolution of an ultra-wide video using a wide-angle video as a Ref video. This yields an 8K video of the scene.

We use the two-stage training strategy used in previous studies [17, 12]. Specifically, we first train the proposed model in a supervised fashion. In this stage, $4\times$ down-sampled ultra-wide and wide-angle videos are treated as LR and Ref inputs, respectively, and the original ultra-wide videos are treated as ground-truth. Subsequently, the pre-trained model is fine-tuned to adapt it to the original-sized videos. In this stage, the original ultra-wide and wide-angle videos serve as LR and Ref inputs, respectively. Due to the absence of ground-truth 8K ultra-wide videos, we use an approximate loss by using the original wide-angle and telephoto videos as pseudo ground-truths.

The details of the first stage are as follows. We train the model to use the $4\times$ downsampled versions of I_t^{UW} and I_t^{Wide} as I_t^{LR} and I_t^{Ref} , respectively, to predict as close I_t^{SR} to the original high-resolution I_t^{UW} as possible. We use the weighted sum of two loss functions, the reconstruction loss and the reference fidelity loss:

$$\ell_{1st} = \ell_{rec} + \beta \ell_{fid}, \quad (11)$$

where β is a weighting constant.

For ℓ_{rec} , we use the same loss as RefVSR, which evaluates the low-frequency and high-frequency components of I_t^{SR} in two terms, respectively, as

$$\ell_{rec} = \|I_{t,blur}^{SR} - I_{t,blur}^{UW}\| + \alpha \sum_i \delta_i(I_t^{SR}, I_t^{UW}), \quad (12)$$

where $I_{t,blur}$ indicates I_t is filtered by 3×3 Gaussian kernels with $\sigma = 0.5$. The second term is called the contextual loss; $\delta_i(X, Y) = \min_j \mathbb{D}(x_i, y_j)$ measures the distance between pixel x_i and the most similar pixel y_j at a perceptual distance \mathbb{D} .

For ℓ_{fid} , we employ the fidelity loss proposed in [17] that uses only a single Ref frame as

$$\ell_{fid}(I_t^{SR}, I_t^{Wide}) = \frac{\sum_i \delta_i(I_t^{SR}, I_t^{Wide}) \cdot c_i}{\sum_i c_i}, \quad (13)$$

where c_i is matching confidence.

The details of the second training stage are as follows. To overcome the performance drop due to the fact that the model is trained on the down-sampled input, we follow the

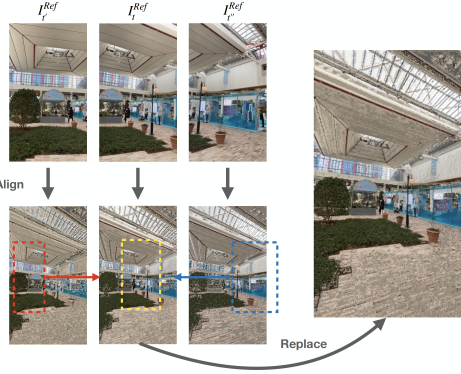


Figure 6: Illustration and example of the test-time feature replacement method of HD frame input.

fine-tuning strategy proposed in [17]. Specifically, we use the original I_t^{UW} and I_t^{Wide} as the LR and Ref inputs, respectively. As there is no ground truth in this case, we 4× down-sample the predicted I_t^{SR} and measure its difference from I_t^{Wide} . In addition, we also use the fidelity loss between I_t^{SR} and the corresponding image I_t^{Tele} of the telephoto video. Therefore, the loss is given as follows:

$$\ell_{2nd} = \|I_{t,blur}^{SR} - I_{t,blur}^{UW}\| + \gamma \ell_{fid}(I_t^{SR}, I_t^{Tele}), \quad (14)$$

where γ is a weighting constant.

4.5. Test-time Feature Replacement

Huang et al. [9] point out an issue with reference-based SR methods: Ref images tend to be misused or underused due to suboptimal feature matching. Lower confidence with high similarity will lead to underuse, whereas high confidence with low similarity will generate wrong textures (i.e., overuse). Furthermore, inaccurate Ref textures will accumulate during the propagation, causing detrimental effects.

We propose a method to cope with these problems. Figure 6 illustrates the background. The images on the left represent the original Ref features (upper row) and their aligned features at three different time steps. Here, we use RGB images for an explanation; we applied the same image warp that applied to the Ref features to their original images. The three Ref features are aligned with the same target image and their reliable regions are shown as boxes. Thus, the region outside the boxes will have erroneous image features due to mismatch. It is hard to train the network to correct these errors in the second training stage for 8K video generation since we do have no ground truths for supervision.

To cope with the difficulty, we propose directly replacing features with low confidence at a time step with features with higher confidence at other time steps. Our Ref feature stream computes the aligned Ref feature \hat{f}_t^{Ref} and its confidence map C_t for alignment, given an LR image I_t^{LR} and a Ref image I_t^{Ref} , as explained in Sec. 4.2. Then we select

Method	Type	PSNR	SSIM	Params
Bicubic	-	26.65	0.800	-
RCAN-pix [21]	SR	31.07	0.915	15.89
IconVSR-pix [3]	VSR	33.80	0.951	7.26
TTSR [20]	R-SR	30.31	0.905	6.7
TTSR-pix [20]	R-SR	30.83	0.911	6.7
DCSR [17]	R-SR	30.63	0.895	5.42
DCSR-pix [17]	R-SR	32.43	0.933	5.42
RefVSR [12]	R-VSR	31.73	0.916	4.78
RefVSR-pix [12]	R-VSR	34.86	0.959	4.78
RefVSR++-small	R-VSR	32.02	0.918	3.27
RefVSR++-small-pix	R-VSR	35.23	0.959	3.27
RefVSR++	R-VSR	32.26	0.925	7.34
RefVSR++-pix	R-VSR	35.90	0.965	7.34

Table 1: Quantitative evaluation of methods on the RealMCVSR dataset. Method column: ‘-pix’ indicates the method is trained with a pixel-based loss; see the texts for details. Type column: SR means single-image SR and VSR means video SR. ‘R-’ indicates it is reference-based. We borrow the PSNR and SSIM values for the methods but ours from [12]. ‘Params’ indicates the number of parameters

a Ref image $I_{t'}^{Ref}$ at different t' in a range $[t - \tau, t + \tau]$ and perform patch matching/alignment with the current LR frame I_t^{LR} , where τ is a hyper-parameter. We denote the resulting features and confidence map by $\hat{f}_{t' \rightarrow t}^{Ref}$ and $C_{t' \rightarrow t}$. We then replace features with low confidence in \hat{f}_t^{Ref} as

$$\hat{f}_{t,ij}^{Ref} = \begin{cases} \hat{f}_{t' \rightarrow t,ij}^{Ref} & \text{if } C_{t' \rightarrow t,ij} > C_{t,ij} \\ \hat{f}_{t,ij}^{Ref} & \text{otherwise,} \end{cases} \quad (15)$$

where ij indicates the image coordinates (i, j) . An example result is shown in the right of Fig. 6; it is obtained by replacing features in the central frame with the other two Ref images. We can see that the generated feature map contains features that are sharper and thus will be more reliable. This method merely reuses the patch-matching module during the test time and does not require additional training.

5. Experimental Results

We evaluate our method using the RealMCVSR dataset [12]. It contains 161 triplets (i.e., ultra-wide, wide-angle, and telephoto, as explained in Sec. 4.4) of HD-resolution (1080×1920) videos captured by iPhone 12 Pro Max equipped with triple cameras. The dataset is divided into training, validation, and testing sets, with 137, 8, and 16 triplets, respectively. We follow [12] for the experimental settings and thus omit the details here; see them in the supplementary. Following previous studies [17, 12], we set the loss weights α , β , and γ to 0.01, 0.05, and 0.1, respectively.

5.1. Quantitative Evaluation

We first quantitatively evaluate the proposed method on the RealMCVSR testset. Following [12], we evaluate meth-

Baseline	Conf	SR	Ref	PSNR
✓				35.19
✓	✓			35.15
✓		✓		35.72
✓			✓	35.62
✓		✓	✓	35.90

Table 2: Results of an ablation test on the two stream feature propagation. See the text for details.

ods on the task of the first training stage, i.e., using $4\times$ down-sampled ultra-wide and wide-angle videos as the LR and Ref inputs, respectively. We evaluated the models trained in the first stage.

Table 1 shows the results. We select several SR methods, i.e., RCAN [21], IconVSR [3], TTSR[20], DCSR [17], and RefVSR [12]. RCAN and IconVSR do not utilize a reference, while others are reference-based methods, which is indicated by ‘R-’ in the type column. Only RefVSR and ours in the reference-based methods are video SR methods. We use two variants of our method with different channel numbers for comparison. The smaller one (with ‘-small’) is 32, and the other is 64. The methods with ‘-pix’ in the method column of Table 1 indicate that they are trained with pixel-based loss alone (i.e., the first term in (11) and (14).)

As with other image restoration/synthesis tasks, SR is affected by the perception-distortion trade-off [2]. Specifically, the models trained with pixel-based loss alone tend to yield better quantitative performance, whereas those trained with additional conceptual loss tend to yield better visual quality. For a fair comparison, we show two results for each of the compared methods. To be specific, RCAN, TTSR, DCSR, and RefVSR employ ℓ_1 loss, whereas IconVSR and ours use the Charbonnier loss [5], for the pixel-based loss. We can see that our method outperforms all the previous methods in each category, even with fewer parameters (i.e., those with ‘-small’). Both types of models are trained and evaluated with $4\times$ downsampled ultra-wide and wide-angle frames. The evaluation is done without test-time replacement method.

As explained above, we use the wide-angle video as Ref inputs and ultra-wide videos as LR inputs. The wide-angle video frame shares only 50% of its FoV with the ultra-wide video frame. Previous studies of reference-based SR found that using Ref frames contributes to improving SR quality inside and outside the overlapped FoV. We compute PSNR and SSIM over the pixels belonging to different FoVs to analyze the dependency in image positions, following [12]. Table 3 shows the results; 0%-50% indicates the overlapped FoV, and 50%- $r\%$ indicates the centered rectangular FoV having $r\%$ area of the frame minus the overlapped (0%-50%) FoV. Like other reference-based methods, our method also suffers from a performance drop in the non-overlapped FoV. Nevertheless, it still yields better performance than

any other method.

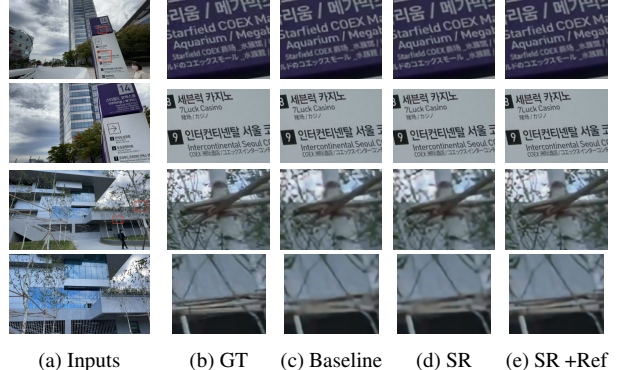


Figure 7: Qualitative comparison of the model variants shown in Table 2. Left most two columns show input ultra-wide and wide-angle images, respectively.

5.2. Qualitative Evaluation

We use generated 8K videos for qualitative comparison. Figure 8 shows selected examples of SR outputs generated by different methods. These are the results of $4\times$ super-resolution from the ultra-wide video inputs in the dataset’s training split. We select one method from each of the different categories in addition to ours, i.e., RCAN [21] (single-image reference SR), BasicVSR++[4] (video SR), and RefVSR[12] and ours (reference video SR). For RCAN and BasicVSR++, we train each using the same training setting as ours on the RealMVS dataset. For RefVSR, we used the pre-trained model released by the authors¹. We can see that the proposed method generates the clearest textures in the overlapped FoV, including correctly reconstructed numbers and alphabets. In image regions outside the overlapped FoV, it yields the most smooth textures with fewer unnatural artifacts.

5.3. Ablation Study

We conduct an ablation test to identify the effectiveness of each component of our method. We experimentally evaluate several variants of the proposed network with different ablated components. Here, we use Charbonnier loss for simplicity. The results are shown in Table 2.

The first variant is a baseline model, the first row in Table 2. It has only our SR feature stream, which performs the basic feature aggregation, where it employs only the optical-flow-based alignment to align the neighboring frames (i.e., $t-1$ and t) and omits the subsequent DCN-based feature alignment/refinement. Its performance (PSNR) is 35.19dB.

The variant in the second row propagates a confidence map and the feature propagation mechanism is identical to

¹<https://github.com/codeslake/RefVSR>

Model	0-50%	50%-60%	50%-70%	50%-80%	50%-90%	50%-100%
Bicubic	25.38/0.757	26.30/0.785	26.42/0.789	26.71/0.798	26.99/0.801	27.29/0.815
RCAN-pix [21]	29.77/0.895	30.69/0.908	30.86/0.910	31.17/0.914	31.50/0.918	31.80/0.921
IconVSR-pix [3]	32.79/0.946	33.43/0.949	33.60/0.950	33.89/0.951	34.19/0.953	34.40/0.953
DCSR-pix [17]	34.90/0.963	31.96/0.927	31.61/0.921	31.58/0.919	31.81/0.921	31.93/0.923
RefVSR-pix [12]	36.14/0.971	34.66/0.959	34.40/0.956	34.34/0.955	34.52/0.955	34.63/0.955
RefVSR++-pix	37.17/0.976	35.99/0.967	35.70/0.965	35.53/0.963	35.63/0.963	35.66/0.962

Table 3: Qualitative results (PSNR/SSIM) measured with centered image regions with different sizes. See texts for details.



Figure 8: Quantitative comparison of different methods on 8K super-resolution.

RefVSR [12], which yields inferior performance. The next variant in the third row is the same network with a single feature stream, but having the full feature alignment mechanism. It improves PSNR by 0.53dB, showing the effectiveness of the DCN-based feature alignment component. The fourth variant is the baseline plus the Ref feature stream. The added Ref feature stream is equipped with the full feature alignment mechanism, unlike the other SR stream. Owing to the fusion of the two features propagating in the two streams, it improves the baseline by 0.43dB in PSNR. This shows the effectiveness of the Ref feature stream and its fusion with the SR stream. The last variant in the fifth row is our full network. The difference from the fourth variant is that the SR feature stream is equipped with the full feature alignment mechanism. It achieves the highest PSNR of 35.90dB. Figure 7 shows qualitative comparisons of proposed components, which agrees with the above quantitative comparisons. More ablation studies are shown in the supplementary.

6. Summary and Conclusion

We have proposed a new method for reference-based video super-resolution (SR) aiming at super-resolving

videos captured by a smartphone’s multi-camera system. The problem is formulated as super-resolving an input low-resolution (LR) video with the help of an input reference (Ref) video. We assume that the Ref video has a narrower FoV and thus contains higher-resolution images of a part of the scene. The proposed method, RefVSR++, extends RefVSR, the existing method for the problem, in two aspects. One is to add a parallel stream for aggregating Ref image features over time in addition to the standard stream aggregating the LR and Ref features over time. This mechanism can derive richer information from the two inputs. The outputs of the two streams are integrated to produce the super-resolution image of the LR input at each time step. The other is an improved mechanism for aligning the LR and Ref features across the neighboring time steps. To further improve the accuracy of feature alignment between LR and Ref images, we propose a novel method that selects better-matched local Ref features according to the alignment confidence and use them to yield better-aligned Ref feature with the LR image. This feature replacement method is designed for 8K SR generation, for which the ground truths for supervision are unavailable at training time. We showed through experiments the effectiveness of RefVSR++.

References

[1] Connelly Barnes, Eli Shechtman, Adam Finkelstein, and Dan B Goldman. Patchmatch: A randomized correspondence algorithm for structural image editing. *ACM Trans. Graph.*, 28(3):24, 2009. 2

[2] Yochai Blau and Tomer Michaeli. The perception-distortion tradeoff. In *Proceedings of the IEEE Conference on Computer Vision and Pattern Recognition*, pages 6228–6237, 2018. 7

[3] Kelvin CK Chan, Xintao Wang, Ke Yu, Chao Dong, and Chen Change Loy. Basicvrs: The search for essential components in video super-resolution and beyond. In *Proceedings of the IEEE Conference on Computer Vision and Pattern Recognition*, 2021. 2, 3, 6, 7, 8

[4] Kelvin CK Chan, Shangchen Zhou, Xiangyu Xu, and Chen Change Loy. Basicvrs++: Improving video super-resolution with enhanced propagation and alignment. In *Proceedings of the IEEE Conference on Computer Vision and Pattern Recognition*, pages 5972–5981, 2022. 2, 3, 4, 7

[5] Pierre Charbonnier, Laure Blanc-Feraud, Gilles Aubert, and Michel Barlaud. Two deterministic half-quadratic regularization algorithms for computed imaging. In *Proceedings of International Conference on Image Processing*, pages 168–172, 1994. 7

[6] Muhammad Haris, Gregory Shakhnarovich, and Norimichi Ukita. Recurrent back-projection network for video super-resolution. In *Proceedings of the IEEE Conference on Computer Vision and Pattern Recognition*, pages 3897–3906, 2019. 2, 3

[7] Yan Huang, Wei Wang, and Liang Wang. Bidirectional recurrent convolutional networks for multi-frame super-resolution. *Advances in Neural Information Processing Systems*, 28, 2015. 3

[8] Yan Huang, Wei Wang, and Liang Wang. Video super-resolution via bidirectional recurrent convolutional networks. *IEEE Transactions on Pattern Analysis and Machine Intelligence*, 40(4):1015–1028, 2017. 2, 3

[9] Yixuan Huang, Xiaoyun Zhang, Yu Fu, Siheng Chen, Ya Zhang, Yan-Feng Wang, and Dazhi He. Task decoupled framework for reference-based super-resolution. In *Proceedings of the IEEE Conference on Computer Vision and Pattern Recognition*, pages 5931–5940, 2022. 1, 2, 4, 6

[10] Takashi Isobe, Xu Jia, Shuhang Gu, Songjiang Li, Shengjin Wang, and Qi Tian. Video super-resolution with recurrent structure-detail network. In *Proceedings of European Conference on Computer Vision*, pages 645–660, 2020. 2

[11] Younghyun Jo, Seoung Wug Oh, Jaeyeon Kang, and Seon Joo Kim. Deep video super-resolution network using dynamic upsampling filters without explicit motion compensation. In *Proceedings of the IEEE Conference on Computer Vision and Pattern Recognition*, pages 3224–3232, 2018. 2

[12] Junyong Lee, Myeonghee Lee, Sunghyun Cho, and Seungyong Lee. Reference-based video super-resolution using multi-camera video triplets. *arXiv preprint arXiv:2203.14537*, 2022. 1, 2, 3, 4, 5, 6, 7, 8

[13] Wenbo Li, Xin Tao, Taian Guo, Lu Qi, Jiangbo Lu, and Jiaya Jia. Mucan: Multi-correspondence aggregation network for video super-resolution. In *European Conference on Computer Vision*, pages 335–351, 2020. 2

[14] Mehdi SM Sajjadi, Raviteja Vemulapalli, and Matthew Brown. Frame-recurrent video super-resolution. In *Proceedings of the IEEE Conference on Computer Vision and Pattern Recognition*, pages 6626–6634, 2018. 2

[15] Wenzhe Shi, Jose Caballero, Ferenc Huszár, Johannes Totz, Andrew P Aitken, Rob Bishop, Daniel Rueckert, and Zehan Wang. Real-time single image and video super-resolution using an efficient sub-pixel convolutional neural network. In *Proceedings of the IEEE Conference on Computer Vision and Pattern Recognition*, pages 1874–1883, 2016. 2

[16] Yapeng Tian, Yulun Zhang, Yun Fu, and Chenliang Xu. Tdan: Temporally-deformable alignment network for video super-resolution. In *Proceedings of the IEEE Conference on Computer Vision and Pattern Recognition*, pages 3360–3369, 2020. 2

[17] Tengfei Wang, Jiaxin Xie, Wenxiu Sun, Qiong Yan, and Qifeng Chen. Dual-camera super-resolution with aligned attention modules. In *Proceedings of the IEEE International Conference on Computer Vision*, pages 2001–2010, 2021. 1, 2, 3, 4, 5, 6, 7, 8

[18] Xintao Wang, Kelvin CK Chan, Ke Yu, Chao Dong, and Chen Change Loy. Edvr: Video restoration with enhanced deformable convolutional networks. In *Proceedings of the IEEE Conference on Computer Vision and Pattern Recognition Workshops*, 2019. 2

[19] Yanchun Xie, Jimin Xiao, Mingjie Sun, Chao Yao, and Kaizhu Huang. Feature representation matters: End-to-end learning for reference-based image super-resolution. In *Proceedings of European Conference on Computer Vision*, pages 230–245, 2020. 1

[20] Fuzhi Yang, Huan Yang, Jianlong Fu, Hongtao Lu, and Baineng Guo. Learning texture transformer network for image super-resolution. In *Proceedings of the IEEE Conference on Computer Vision and Pattern Recognition*, pages 5791–5800, 2020. 2, 3, 6, 7

[21] Yulun Zhang, Kunpeng Li, Kai Li, Lichen Wang, Bineng Zhong, and Yun Fu. Image super-resolution using very deep residual channel attention networks. In *Proceedings of European Conference on Computer Vision*, 2018. 6, 7, 8

[22] Zhifei Zhang, Zhaowen Wang, Zhe Lin, and Hairong Qi. Image super-resolution by neural texture transfer. In *Proceedings of the IEEE Conference on Computer Vision and Pattern Recognition*, pages 7982–7991, 2019. 1, 2, 3

[23] Haitian Zheng, Mengqi Ji, Lei Han, Ziwei Xu, Haoqian Wang, Yebin Liu, and Lu Fang. Learning cross-scale correspondence and patch-based synthesis for reference-based super-resolution. In *Proceedings of British Machine Vision Conference*, 2017. 1

[24] Haitian Zheng, Mengqi Ji, Haoqian Wang, Yebin Liu, and Lu Fang. Crossnet: An end-to-end reference-based super resolution network using cross-scale warping. In *Proceedings of the European Conference on Computer Vision*, pages 88–104, 2018. 1, 2, 3

[25] Xiaobin Zhu, Zhuangzi Li, Xiao-Yu Zhang, Changsheng Li, Yaqi Liu, and Ziyu Xue. Residual invertible spatio-

temporal network for video super-resolution. In *Proceedings of the AAAI Conference on Artificial Intelligence*, pages 5981–5988, 2019. 2